AMSE JOURNALS-AMSE IIETA publication-2017-Series: Advances C; Vol. 72; N°4; pp 292-311
Submitted July 2017; Revised Oct. 30, 2017, Accepted Nov.15, 2017
https://doi.org/10.18280/ama_c.720407

Comparative Analysis between the Rotor Flux Oriented Control and Backstepping Control of a Double Star Induction Machine (DSIM) under Open-Phase Fault

*N. Layadi, **S. Zeghlache, *T. Benslimane, ***F. Berrabah

* Laboratory of Electrical Engineering, Department of Electrical Engineering, Faculty of Technology, University Mohamed Boudiaf of M'sila, BP 166, Ichbilia 28000, Algeria (masterbba2015@gmail.com, bens082002@yahoo.fr)

** Laboratory of Analysis of Signals and Systems, Department of Electronics, Faculty of Technology, University Mohamed Boudiaf of M'sila, BP 166, Ichbilia 28000, Algeria (zegsam5@gmail.com)

*** Department of Electrical Engineering, Faculty of Technology, University Mohamed Boudiaf of M'sila, BP 166, Ichbilia 28000, Algeria (Fouadberrabah1@gmail.com)

Abstract

This paper proposes a fault tolerant control (FTC) for double star induction machine (DSIM) of *4.5 kW* under open-phase fault (OPF) within the first stator. The DSIM is fed by two three-phase voltage source inverters (VSI) using pulse width modulation (PWM) control strategies. This FTC is based on backstepping control (BSC) without needing an additional hardware. The proposed control design is based on Lyapunov stability theory and using an estimator of rotor flux. A comparative study is made between the proposed FTC and rotor field oriented control (RFOC) based on regulators proportional-integral (PI). Simulation results via Matlab/Simulink are presented to compare the performance of the system using these two control scheme. Obtained results show that the backstepping FTC has a fast dynamic, better tracking performance and better robustness against the OPF.

Key words

Double Star Induction Machine, Backstepping Control, Open-Phase Fault, Rotor Field Oriented Control.

1. Introduction

In the last few years many important researches were interested to study the fault tolerant control (FTC) of the induction motor (IM) in order to improve its performances under faulty state. Starting from (Belhamdi, 2011), in that paper a sliding mode control of asynchronous machine under rotor bars defect is proposed. (Belhamdi, 2013) develop a fuzzy logic control of IM under defective rotor bars. The same authors (Belhamdi, 2015) present a design of a fuzzy logic type-2 controller based on direct torque control (DTC) strategy for IM under broken bars. All simulation results of these works show that the FTC is very essential to keep acceptable performances such as speed and electromagnetic torque in an IM under rotor faults.

Among the multi-phase machine the double star induction machine (DSIM) is the most used in different fields of industry that need high power such as electric vehicles, locomotive traction, naval applications and other fields in which the safety conditions required such as aerospace and wind energy systems. The significant number of phases that DSIM owns allows it to have power segmentation, lower torque ripple, reduced rotor harmonics and many other advantages (Kortas, 2017). Therefore, it is very beneficial to apply a control strategy which maintains these advantages in case of open-phase fault.

The Backstepping control is confirmed by experimental results and has been successfully applied to three-phase induction motor (Ameid, 2017), five-phase induction motor (Echeikh, 2016) and six-phase induction motor (Rastegar Fatemi, 2014). This control structure can ensures overall closed loop stabilization in presence of uncertain parameters. The effectiveness of the proposed control is proved under crucial operating state.

Open-phase fault (OPF) operation of the multi-phase IM has been recently analyzed starting from (Bermúdez, 2015, 2017) where authors proved the performances of DTC method compared to RFOC of five-phase IM drive with open-phase fault. In (Duran, 2017) a Six-phase induction motor drives is studied, in that paper researchers developed a detection method of OPF using secondary currents (named x-y currents) which distinguish the multi-phase machines. Experimental results affirm the robustness and fast fault detection of the proposed method.

This paper present comparison studies between the rotor flux oriented control and a FTC based on non-linear backstepping strategy accompanied by simulation results and analysis to prove the efficiency and robustness satisfactory of the proposed control.

This paper is organized as follow in section 2 a modeling of DSIM is presented. A rotor flux estimator is calculated in section 3. Section 4 presents the rotor field oriented control. In section 5 an open-phase fault is simulated using MATLAB/SIMULINK. The backstepping control design is included in section 6, in this section the stability of the closed loop system is verified by

Lyapunov stability theory. Simulation results and comparison between the two approaches are given in section 7. The last section is reserved for conclusion and reference list.

2. DSIM modeling

DSIM has two stators shifted by an electrical angle and mobile squirrel cage rotor composed by three phases. Each star is composed by three immovable windings. The Fig. 1 shows an explicit schematic which represents the stator and rotor windings. The windings series (S_{a1}, S_{b1}, S_{c1}), (S_{a2}, S_{b2}, S_{c2}), (R_a, R_b, S_c) represent stator 1, stator 2 and rotor, respectively, α is the angle shift between the two stators, θ is the angle between rotor and stator 1. In this research we choose $\alpha = 30^0$ with accordance to (Rahali, 2017).

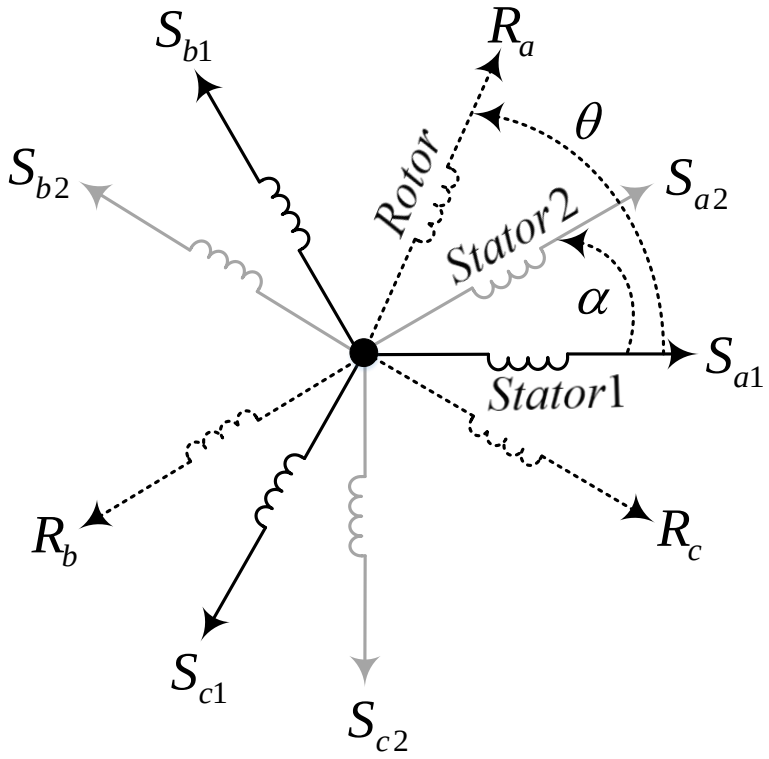

Fig.1. DSIM windings representation

2.1 DSIM mathematical model

The DSIM dynamic model in the synchronous Park reference frame is given as (Rahali, 2017):

A. Electrical equations

- First stator:

$$\begin{cases} v_{sd1} = R_{s1} i_{sd1} + \dfrac{d}{dt}\varphi_{sd1} - \omega_s \varphi_{sq1} \\ v_{sq1} = R_{s1} i_{sq1} + \dfrac{d}{dt}\varphi_{sq1} + \omega_s \varphi_{sd1} \end{cases} \quad (1)$$

- Second stator:

$$\begin{cases} v_{sd2} = R_{s1} i_{sd2} + \dfrac{d}{dt}\varphi_{sd2} - \omega_s \varphi_{sq2} \\ v_{sq2} = R_{s2} i_{sq2} + \dfrac{d}{dt}\varphi_{sq2} + \omega_s \varphi_{sd2} \end{cases} \quad (2)$$

- Rotor :

$$\begin{cases} 0 = R_r i_{rd} + \dfrac{d}{dt}\varphi_{rd} - \omega_{gl} \varphi_{rq} \\ 0 = R_r i_{rq} + \dfrac{d}{dt}\varphi_{rq} + \omega_{gl} \varphi_{rd} \end{cases} \quad (3)$$

B. Flux equations

- First stator:

$$\begin{cases} \varphi_{sd1} = L_{s1} i_{sd1} + L_m (i_{sd1} + i_{sd2} + i_{rd}) \\ \varphi_{sq1} = L_{s1} i_{sq1} + L_m (i_{sq1} + i_{sq2} + i_{rq}) \end{cases} \quad (4)$$

- Second stator:

$$\begin{cases} \varphi_{sd2} = L_{s2} i_{sd2} + L_m (i_{sd1} + i_{sd2} + i_{rd}) \\ \varphi_{sq2} = L_{s2} i_{sq2} + L_m (i_{sq1} + i_{sq2} + i_{rq}) \end{cases} \quad (5)$$

- Rotor:

$$\begin{cases} \varphi_{rd} = L_r i_{rd} + L_m (i_{sd1} + i_{sd2} + i_{rd}) \\ \varphi_{rq} = L_r i_{rq} + L_m (i_{sq1} + i_{sq2} + i_{rq}) \end{cases} \quad (6)$$

C. Mechanical equation (Meroufel, 2017)

$$\frac{d}{dt}\Omega_r = T_e - T_L - K_f \Omega_r \quad (7)$$

The electromagnetic torque equation is given by:

$$T_e = p\frac{L_m}{L_m + L_r}[\varphi_{rd}(i_{sq1} + i_{sq2}) - \varphi_{rq}(i_{isd1} + i_{sd2})] \quad (8)$$

2.2 State equations

In order to design easily the proposed backstepping controller, we choose the following state representation of DSIM in the d-q oriented axes:

$$\dot{x} = f(x) + Bv + DT_L \quad (9)$$

Where $\dot{x}$ is the state vector given by:

$\dot{x} = [x_1 \quad x_2 \quad x_3 \quad x_4 \quad x_5 \quad x_6]^T = [i_{sd1} \quad i_{sq1} \quad i_{sd2} \quad i_{sq2} \quad \omega_r \quad \varphi_r]^T$, $v = [v_{sd1} \quad v_{sq1} \quad v_{sd2} \quad v_{sq2}]^T$ is the vector control and $[\omega_r \quad \varphi_r]^T$ is the output of the system. With:

$$B = \begin{bmatrix} b_1 & 0 & 0 & 0 & 0 & 0 \\ 0 & b_1 & 0 & 0 & 0 & 0 \\ 0 & 0 & b_2 & 0 & 0 & 0 \\ 0 & 0 & 0 & b_2 & 0 & 0 \end{bmatrix}^T, \quad b_1 = \frac{1}{L_{s1}}, b_2 = \frac{1}{L_{s2}}, D = [0 \quad 0 \quad 0 \quad 0 \quad d \quad 0]^T, \; d = -\frac{p}{J}.$$

f(x) is a vector which given by the following system of equations :

$$\begin{cases} f_1(x) = a_1x_1 + a_2x_2 + a_3 \\ f_2(x) = a_4x_1 + a_1x_2 + a_5 \\ f_3(x) = a_6x_3 + a_2x_4 + a_7 \\ f_4(x) = a_4x_3 + a_6x_4 + a_8 \\ f_5(x) = a_9(x_2 + x_4) + a_{10}x_5 + a_{11}T_L \\ f_6(x) = a_{12}(x_1 + x_3) + a_{13}x_6 \end{cases} \quad (10)$$

The components of *f(x)* are expressed according to the machine parameters as follows:

$$\begin{cases} a_1 = -\dfrac{R_{s1}}{L_{s1}}, a_2 = \omega_s^*, a_3 = \dfrac{\omega_s^* T_r \varphi_r^* \omega_{gl}^*}{L_{s1}}, a_4 = -\omega_s^* \\ a_5 = -\dfrac{\omega_s^* \varphi_r^*}{L_{s1}}, a_6 = -\dfrac{R_{s2}}{L_{s2}}, a_7 = \dfrac{\omega_s^* T_r \varphi_r^* \omega_{gl}^*}{L_{s2}} \\ a_8 = -\dfrac{\omega_s^* \varphi_r^*}{L_{s2}}, a_9 = \dfrac{p^2 L_m \varphi_r^*}{J(L_m + L_r)}, a_{10} = -\dfrac{K_f}{J} \\ a_{11} = -\dfrac{p}{J}, a_{12} = \dfrac{L_m R_r}{L_m + L_r}, a_{13} = -\dfrac{R_r}{L_m + L_r} \end{cases} \quad (11)$$

3. Rotor Flux Estimator:

From equation (9) we have the state equation of rotor flux:

$$\dot{x}_6 = \dot{\varphi}_r = f_6(x) = a_{12}(x_1 + x_3) + a_{13} x_6 = \frac{L_m R_r}{L_m + L_r}(i_{sd1} + i_{sd2}) - \frac{R_r}{L_m + L_r}\varphi_r \quad (12)$$

By applying Laplace transform, the transfer function of (12) is:

$$\varphi_r = \frac{L_m R_r}{s(L_m + L_r) + R_r}(i_{sd1} + i_{sd2}) = \frac{L_m R_r}{s(L_m + L_r) + R_r} i_{sd} \quad (13)$$

Where: s is the Laplace coefficient.

From equation (13) we can establish a control loop based on a PI controller that estimate the rotor flux as shown in Fig. 2.

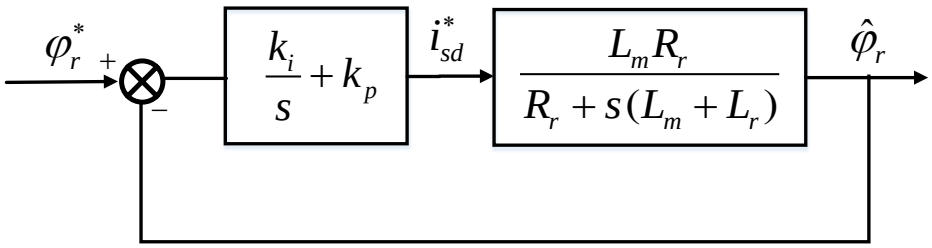

Fig. 2. PI controller of rotor flux estimator.

The PI parameters are given by:

$$\begin{cases} k_i = \dfrac{L_m + L_r}{2R_m L_m T_r} \\ k_p = \dfrac{1}{2L_m T_r} \end{cases} \tag{14}$$

4. Rotor Field Oriented Control

This control technique consists to achieve the decoupling between flux and electromagnetic torque as in DC machines by preserving the quadrature component of the flux null and the direct flux equals to the reference, we have the following equation (Tir, 2017 and Lekhchine, 2014):

$$\begin{cases} \varphi_{rd} = \varphi_r^* \\ \varphi_{rq} = 0 \end{cases} \tag{15}$$

Using systems of equations (3), (8) and (15), the references values of slip speed and torque can be written as:

$$\omega_{gl}^* = \frac{R_r L_m}{(L_m + L_r)\varphi_r^*}(i_{sq1}^* + i_{sq2}^*) \tag{16}$$

$$T_e = p\frac{L_m}{(L_m + L_r)}\varphi_r^*(i_{sq1}^* + i_{sq2}^*) \tag{17}$$

Assuming that

$$\begin{cases} i_{sq1}^* + i_{sq2}^* = i_{sq} \\ i_{sd1}^* + i_{sd2}^* = i_{sd} \end{cases} \tag{18}$$

And

$$\begin{cases} i_{sq1}^* = i_{sq2}^* \\ i_{sd1}^* = i_{sd2}^* \end{cases} \tag{19}$$

After the decoupling between the quadrature stator currents and the reference flux in the electromagnetic torque expression presented in equation (17), the reference values of stator voltages are given as follow:

$$\begin{cases} v_{sd1}^{*} = v_{sd1} - v_{sd1c} \\ v_{sq1}^{*} = v_{sq1} + v_{sq1c} \\ v_{sd2}^{*} = v_{sd2} - v_{sd2c} \\ v_{sq2}^{*} = v_{sq2} + v_{sq2c} \end{cases} \tag{20}$$

With

$$\begin{cases} v_{sd1c} = \omega_s^{*} \left(L_{s1} i_{sq1} + T_r \varphi_r^{*} \omega_{gl}^{*} \right) \\ v_{sq1c} = \omega_s^{*} \left(L_{s1} i_{sd1} + \varphi_r^{*} \right) \\ v_{sd2c} = \omega_s^{*} \left(L_{s2} i_{sq2} + T_r \varphi_r^{*} \omega_{gl}^{*} \right) \\ v_{sq2c} = \omega_s^{*} \left(L_{s2} i_{sd2} + \varphi_r^{*} \right) \end{cases} \tag{21}$$

And

$$\begin{cases} v_{sd1} = R_{s1} i_{sd1} + L_{s1} \dfrac{d}{dt} i_{sd1} \\ v_{sq1} = R_{s1} i_{sq1} + L_{s1} \dfrac{d}{dt} i_{sq1} \\ v_{sd2} = R_{s2} i_{sd2} + L_{s2} \dfrac{d}{dt} i_{sd2} \\ v_{sq2} = R_{s2} i_{sq2} + L_{s2} \dfrac{d}{dt} i_{sq2} \end{cases} \tag{22}$$

For perfect decoupling, a regulator proportional-integral (PI) is added in order to adjust the stator currents, the outputs of these regulation loops are stator voltages. In this control scheme we used a direct method of speed control which requires a good knowledge of the flux module and its phase. Thus, we use a rotor flux estimator as presented in section 3.

5. Simulation of Open-Phase Fault in MATLAB/SIMULINK

When an open-phase fault occurs, the performance of the DSIM changes, the system becomes asymmetrical and the current in the faulty phase equals zero. To simulate easily an open-phase fault we force i_a to zero for this we must set $i_\alpha = 0$ after making a d-q / α-β transformation as shown in Fig. 3.

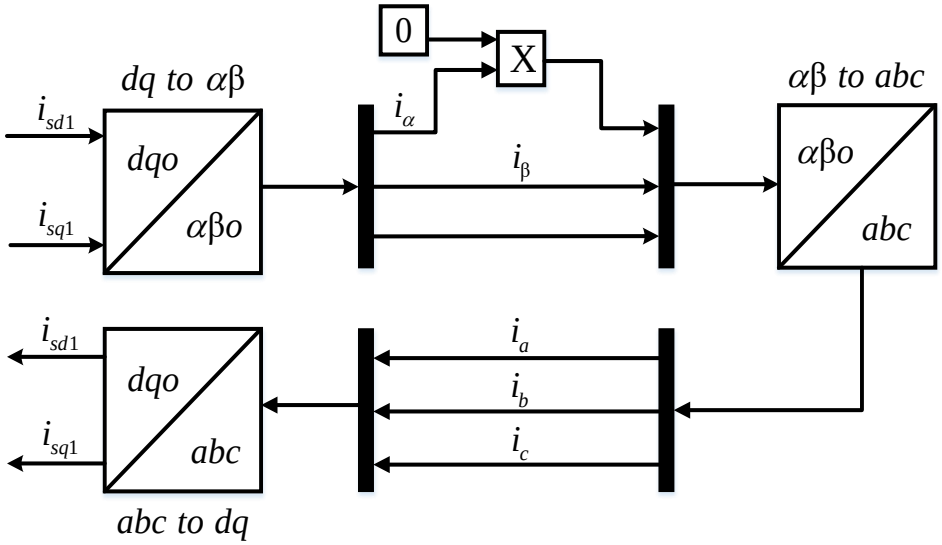

Fig.3. Simulation of an open-phase using Simulink/Matlab

6. Backstepping Control Design

6.1 First Step: Speed and Flux Control

The aim of this step is to lead the vector $[\omega_r \quad \varphi_r]^T$ to its desired reference $[\omega_r^* \quad \varphi_r^*]^T$. This will produce two tracking errors:

$$\begin{bmatrix} e_1 \\ e_2 \end{bmatrix} = \begin{bmatrix} x_5^* - x_5 \\ x_6^* - x_6 \end{bmatrix} = \begin{bmatrix} \omega_r^* - \omega_r \\ \varphi_r^* - \varphi_r \end{bmatrix} \tag{23}$$

The dynamics of tracking errors are:

$$\begin{bmatrix} \dot{e}_1 \\ \dot{e}_2 \end{bmatrix} = \begin{bmatrix} \dot{x}_5^* - \dot{x}_5 \\ \dot{x}_6^* - \dot{x}_6 \end{bmatrix} = \begin{bmatrix} \dot{\omega}_r^* - \dot{\omega}_r \\ \dot{\varphi}_r^* - \dot{\varphi}_r \end{bmatrix} \tag{24}$$

$$\begin{bmatrix} \dot{e}_1 \\ \dot{e}_2 \end{bmatrix} = \begin{bmatrix} \dot{\omega}_r^* - a_9 (x_2 + x_4) - a_{10} x_5 - a_{11} T_L \\ \dot{\varphi}_r^* - a_{12} (x_1 + x_3) - a_{13} x_6 \end{bmatrix} \tag{25}$$

The first Lyapunov function linked to the rotor flux and speed errors is defined by:

$$V_1 = \frac{(e_1^2 + e_2^2)}{2} \tag{26}$$

The dynamic of Lyapunov function is:

$$\dot{V}_1 = e_1\dot{e}_1 + e_2\dot{e}_2 \tag{27}$$

From equation (25), $\dot{V}_1$ can be written as follows:

$$\dot{V}_1 = e_1\left(\dot{\omega}_r^* - a_9(x_2 + x_4) - a_{10}x_5 - a_{11}T_L\right) + e_2\left(\dot{\varphi}_r^* - a_{12}(x_1 + x_3) - a_{13}x_6\right) \tag{28}$$

In order to have the derivative of Lyapunov function negative definite we pose:

$$\begin{cases} \dot{e}_1 = -G_1e_1 \\ \dot{e}_2 = -G_2e_2 \end{cases} \tag{29}$$

Where: G_1 and G_2 are the positives gains which adjust the dynamic of closed loop.

By replacing system of equations (29) into system of equations (27) we obtain:

$$\dot{V}_1 = -G_1e_1^2 - G_2e_2^2 < 0 \tag{30}$$

In other hand the systems of equations (25) and (29) generate the following equalities:

$$\begin{cases} \dot{\omega}_r^* - a_9(x_2 + x_4) - a_{10}x_5 - a_{11}T_L = -G_1e_1 \\ \dot{\varphi}_r^* - a_{11}(x_1 + x_3) - a_{12}x_6 = -G_2e_2 \end{cases} \tag{31}$$

The two stators are identical, so we put:

$$\begin{cases} x_2 + x_4 = i_{sq1} + i_{sq2} = i_{sq}^* \\ x_1 + x_3 = i_{sd1} + i_{sd2} = i_{sd}^* \end{cases} \tag{32}$$

By Substituting system of equations (32) into equations (31) we found the intermediate control represented by the following reference currents:

$$\begin{cases} i_{sd}^{*} = \dfrac{1}{a_{11}}\left[\dot{\varphi}_r^{*} - a_{12}x_6 + G_2 e_2\right] \\ i_{sq}^{*} = \dfrac{1}{a_8}\left[\dot{\omega}_r^{*} - a_9 x_5 - a_{10}T_L + G_1 e_1\right] \end{cases} \tag{33}$$

6.2 Second Step: Currents Control

In this stage the control law will be established by adjusting the four stator currents: i_{sd1}, i_{sq1}, i_{sd2}, i_{sq2} generated by the first step so, we also specify their error signals:

$$\begin{cases} e_3 = i_{sd1}^{*} - i_{sd1} = x_1^{*} - x_1 \\ e_4 = i_{sq1}^{*} - i_{sq1} = x_2^{*} - x_2 \\ e_5 = i_{sd2}^{*} - i_{sd2} = x_3^{*} - x_3 \\ e_6 = i_{sq2}^{*} - i_{sq2} = x_4^{*} - x_4 \end{cases} \tag{34}$$

The time derivate of equation (34) gives:

$$\begin{cases} \dot{e}_3 = \dot{x}_1^{*} - \dot{x}_1 = \dfrac{d}{dt} i_{sd1}^{*} - \dfrac{d}{dt} i_{sd1} \\ \dot{e}_4 = \dot{x}_2^{*} - \dot{x}_2 = \dfrac{d}{dt} i_{sq1}^{*} - \dfrac{d}{dt} i_{isq1} \\ \dot{e}_5 = \dot{x}_3^{*} - \dot{x}_3 = \dfrac{d}{dt} i_{sd2}^{*} - \dfrac{d}{dt} i_{sd2} \\ \dot{e}_6 = \dot{x}_4^{*} - \dot{x}_4 = \dfrac{d}{dt} i_{sq2}^{*} - \dfrac{d}{dt} i_{sq2} \end{cases} \tag{35}$$

By substituting $\dot{x}_1$, $\dot{x}_2$, $\dot{x}_3$, $\dot{x}_4$ with their expressions from equations (9), the dynamical equations for the error signals becomes as follow:

$$\begin{bmatrix} \dot{e}_3 \\ \dot{e}_4 \\ \dot{e}_5 \\ \dot{e}_6 \end{bmatrix} = \begin{bmatrix} \dot{x}_1^{*} - a_1 x_1 - a_2 x_2 - a_3 - b_1 v_{sd1} \\ \dot{x}_2^{*} - a_4 x_1 - a_1 x_2 - a_5 - b_1 v_{sq1} \\ \dot{x}_3^{*} - a_6 x_3 - a_2 x_4 - a_7 - b_2 v_{sd2} \\ \dot{x}_4^{*} - a_4 x_3 - a_6 x_4 - a_8 - b_2 v_{sq2} \end{bmatrix} \tag{36}$$

Stability analysis of the system is done by the global Lyapunov function which is defined by:

$$V_2 = V_1 + \frac{(e_3^2 + e_4^2 + e_5^2 + e_6^2)}{2} \tag{37}$$

The derivative is then written as:

$$\dot{V}_2 = \dot{V}_1 + \dot{e}_3 e_3 + \dot{e}_4 e_4 + \dot{e}_5 e_5 + \dot{e}_6 e_6 \tag{38}$$

The system global stability is achieved if only $\dot{V}_2$ definite negative therefore $\dot{e}_3$, $\dot{e}_4$, $\dot{e}_5$, $\dot{e}_6$ are chosen as in the first step:

$$\begin{cases} \dot{e}_3 = -G_3 e_3 \\ \dot{e}_4 = -G_4 e_4 \\ \dot{e}_5 = -G_5 e_5 \\ \dot{e}_6 = -G_6 e_6 \end{cases} \tag{39}$$

G_3, G_4, G_5, G_6 are positives constants that fix the closed-loop dynamic. This also we lead us to:

$$\dot{V}_2 = -G_1 e_1^2 - G_2 e_2^2 - G_3 e_3^2 - G_4 e_4^2 - G_5 e_5^2 - G_6 e_6^2 < 0 \tag{40}$$

Using systems of equations (36) and (39), we obtain the actual control represented by the following components of stator voltages:

$$\begin{cases} v_{sd1} = \dfrac{1}{b_1}\left[\dot{x}_1^* - a_1 x_1 - a_2 x_2 - a_3 + G_3 e_3\right] \\ v_{sq1} = \dfrac{1}{b_1}\left[\dot{x}_2^* - a_4 x_1 - a_1 x_2 - a_5 + G_4 e_4\right] \\ v_{sd2} = \dfrac{1}{b_2}\left[\dot{x}_3^* - a_6 x_3 - a_2 x_4 - a_7 + G_5 e_5\right] \\ v_{sq2} = \dfrac{1}{b_2}\left[\dot{x}_4^* - a_4 x_3 - a_6 x_4 - a_8 + G_6 e_6\right] \end{cases} \tag{41}$$

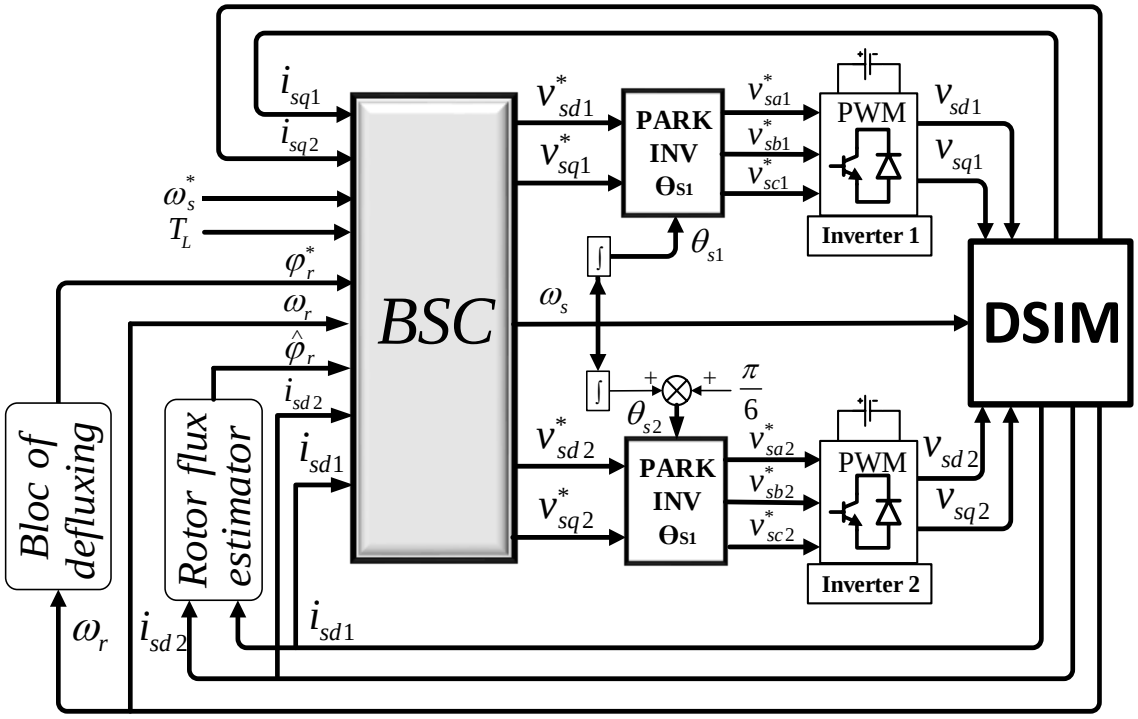

Fig.4. Speed control scheme with BSC

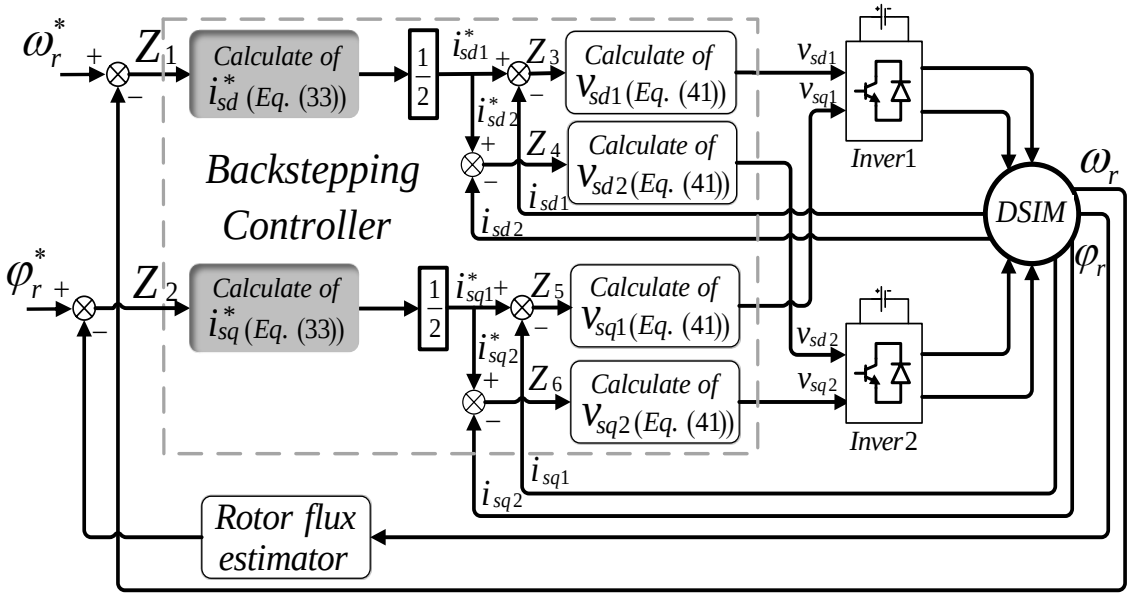

Fig.5. Backstepping control design

7. Simulation results and comparisons

In order to verify the effectiveness and robustness of the proposed control compared to RFOC in faulty operation, a test of open-phase fault was introduced on RFOC and backstepping structure. The DSIM studied in this paper is fed by two PWM-VSI where its parameters are as follows: Voltage: *230-380 V*, Power: *4.5 kW*, frequency *f = 50 Hz*. The nominal electrical and

mechanical parameters are given in appendix. The reference speed is fixed to *200 rd/s*. The DSIM is starting in balanced operation, a load torque (*14 N.m*) is applied at *t=2sec* and followed by open-phase fault in the first stator which occurs at *t=3sec*. This test is done by simulation using Matlab/Simulink environment.

7.1 Healthy Case (pre- fault)

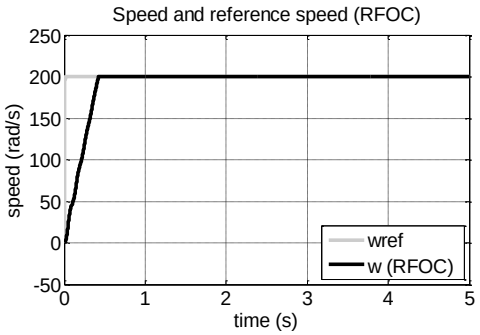

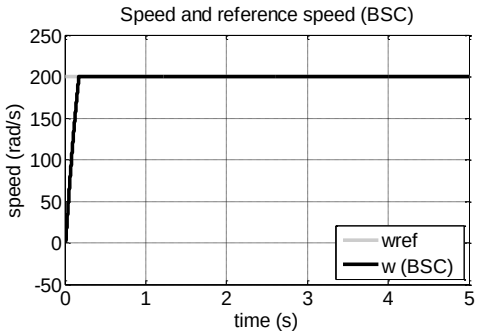

(a)

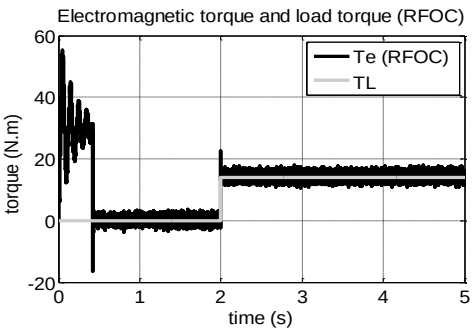

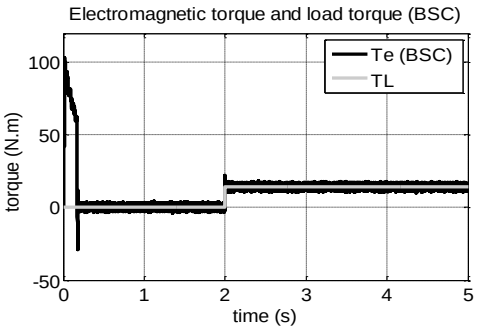

(b)

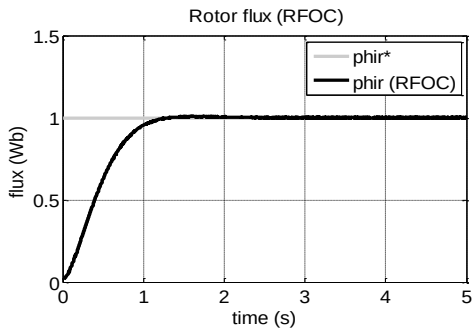

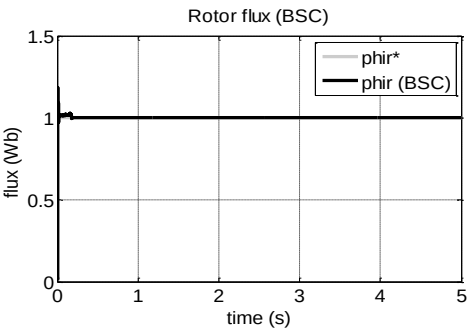

(c)

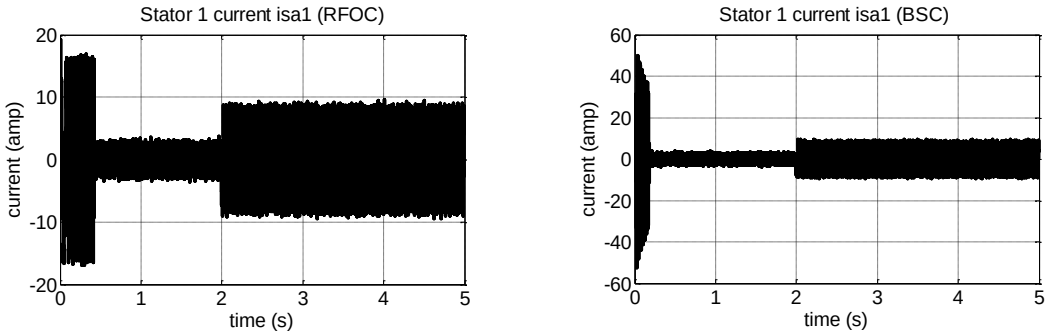

(d)

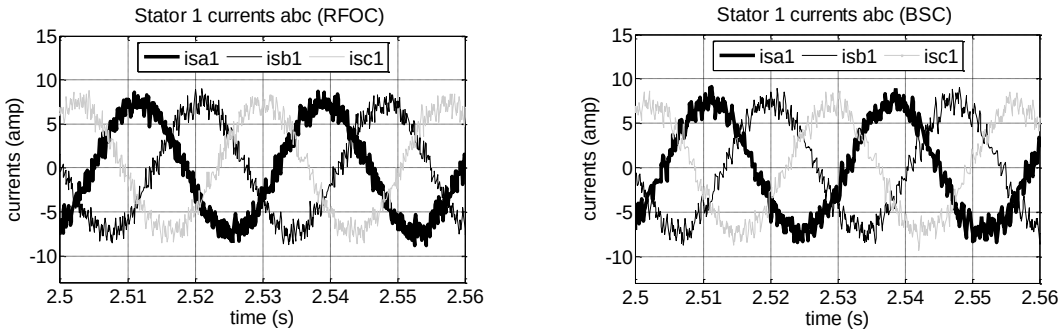

(e)

Fig.6. Simulation results of RFOC and BSC in healthy state

Fig. 6 shows the performances of the system in steady and transient-states for a balanced DSIM (un-faulty operation) starting by RFOC which is based on proportional-integral (PI) on the left side and the non-linear BSC based on Lyapunov theory on the right side. Fig. 6.a shows the speed responses for the two control methods, in both signals the speed follows its reference value with negligible overtake and without oscillations, but it is clearly shows that the proposed BSC has faster response than RFOC and imposes a short transient regime with a response time equals *0.17 sec*, while for RFOC, the response time equal to *0.42 sec*, the proposed control also provides better stability with the smallest average static error. No ripples in the electromagnetic signals as illustrated in Fig. 6.b proving that both control schemes are able to surmount the external load torque rejection. At start-up the electromagnetic torque presents oscillations and a peak of *55 N.m*, *103 N.m* for RFOC and BSC, respectively. After the transient regime, the torque compensates the friction losses and load torque. Fig. 6.c show that the two control methods are suitable to lead the flux to it desired reference but BSC has the fastest dynamic response than RFOC. Finally, Fig. 6.d and Fig. 6.e show the behavior of the three currents i_a, i_b and i_c of the first stator which have the same amplitude and their shape is sinusoidal affected by the switching frequency generated by the inverter, during the dynamic state, the DSIM consumes very important currents, when inserting the load, the amplitude of currents reach *9 A* for both control

techniques. The obtained results in a pre-fault state summarize and reflect the response swiftness of BSC compared to the RFOC.

7.2 Open-phase fault Case (post- fault)

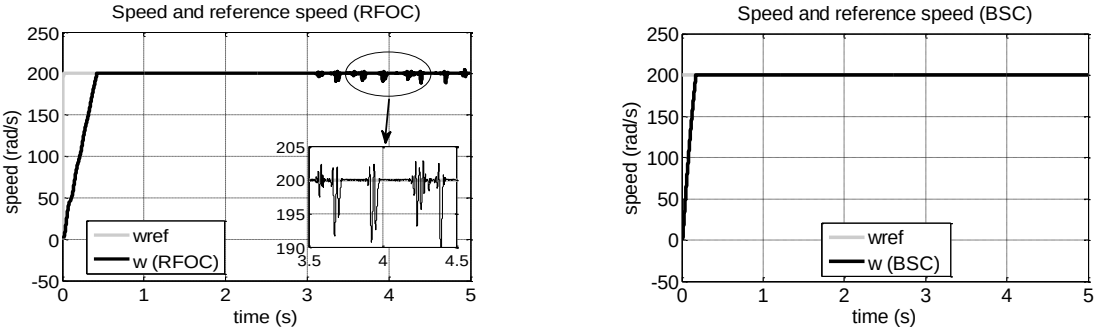

(a)

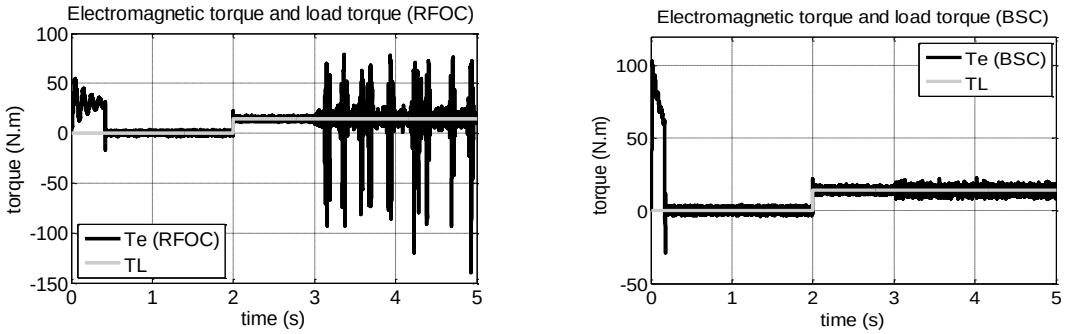

(b)

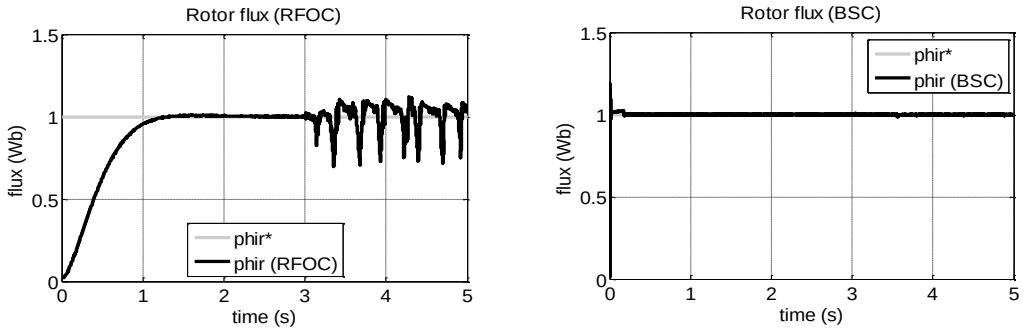

(c)

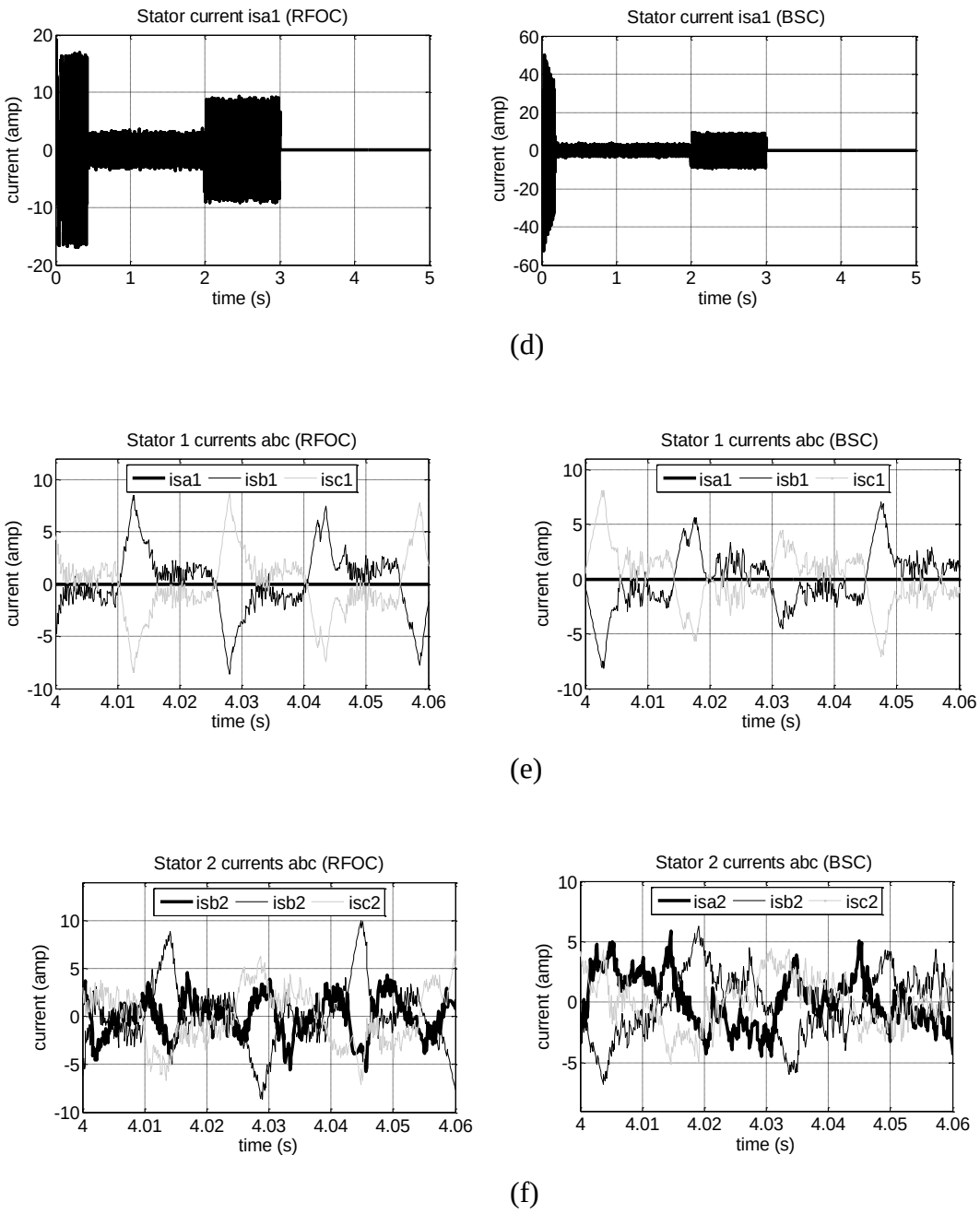

Fig.7. Simulation results of RFOC and BSC under open-phase fault

In this case the first phase is disconnected at *t=3 sec*, this fault is immediately detected. The performances of DSIM during post-fault operation are shown in Fig. 7. The machine is driven at *200 rd/s* before and after the fault occurs, with constant load torque of *14 N.m*. It is important to notice the degradation of the speed tracking with RFOC method in steady state after the fault occurrence. However, when using the proposed controller, rotor speed oscillations are disappeared (see Fig. 7.a). In Fig. 7.b, important ripples in the electromagnetic torque can be seen with RFOC where the maximum positive ripple reaches *+80 N.m* and the maximum negative

ripple reached *-140 N.m*, on the other hand BSC reduces the torque oscillations considerably. We mention that the torque ripple magnitude is also affected by the switching frequency caused by the two three-phase VSI. In Fig. 7.c, with the proposed control, the rotor flux track its reference value properly even under OPF, on the other hand, the flux response of RFOC presents ripples after *t=3sec*. In Fig. 7.d a horizontal line is distinctly observed with both controllers because the current i_{sa1} circulating in the disconnected phase equals zero. After the fault occurs the two healthy phases currents stay symmetrical (equal phase current magnitudes with an inverse sign) and their amplitudes decrease, this is confirmed by the zoom-in of the three currents (i_{sa1}, i_{sb1}, i_{sc1}) circulating in the three windings of the first stator during the open-phase fault as shown in Fig. 7.e. The last Fig. 7.f shows the evolution of the second stator currents using RFOC and BSC controllers during the open-phase fault. The deformation of these three signals expresses the compensation of phase-loss by the stator 2. It can be seen from these simulation results that the backstepping control ensures satisfactory robustness against the open-phase fault while the RFOC is unable to master the unbalanced machine properly. The proposed scheme in this paper evidently is more efficiency than the RFOC in the two operating cases.

8. Conclusion

An accurate and simple fault tolerant control based on backstepping strategy of double star induction machine has been presented. Simulation results shown the robustness of the proposed controller during the faulty operation compared to RFOC, concluding that the speed and flux references are kept after the fault occurrence with good tracking and the oscillations that appeared in electromagnetic torque can be efficiently decreases with overall rejection of the load torque disturbance. The proposed control can be used in crucial industrial applications. The performances obtained prove that the proposed BSC is more effective than RFOC for directing the open-phase mode operating.

References

1. S. Belhamdi and A. Goléa, Sliding Mode Control of Asynchronous Machine Presenting Defective Rotor Bars, AMSE Journals, Series Advances C, vol. 66, no. 1/2, pp. 39-49, 2011.
2. S. Belhamdi and A. Goléa, Fuzzy logic Control of Asynchronous Machine Presenting Defective Rotor Bars, AMSE Journals, Series Advances C, vol. 68, no. 1/2, pp. 54-63, 2013.
3. S. Belhamdi and A. Goléa, Direct Torque Control for Induction Motor with broken bars using Fuzzy Logic Type-2, AMSE Journals, Series Advances C, vol. 70, no. 1, pp. 15-28, 2015.

4. I. Kortas, A. Sakly and M. F. Mimouni, Optimal vector control to a double-star induction motor, Energy, vol. 131, pp. 279-288, 2017.
5. T. Ameid, A. Menacer, H. Talhaoui, I. Harzelli and A. Ammar, Backstepping control for induction motor drive using reduced model in healthy state: Simulation and experimental study, 2017 6th International Conference on Systems and Control (ICSC), Batna, Algeria, May 2017, Proc. pp 162-167.
6. H. Echeikh, R. Trabelsi, A. Iqbal, N. Bianchi and M. F. Mimouni, Comparative study between the rotor flux oriented control and non-linear backstepping control of a five-phase induction motor drive–an experimental validation, IET Power Electronics, vol. 9, no. 13, pp. 2510-2521, 2016.
7. H. Echeikh, R. Trabelsi, A. Iqbal, N. Bianchi and M. F. Mimouni, Non-linear backstepping control of five-phase IM drive at low speed conditions–experimental implementation, ISA transactions, vol. 65, pp. 244-253, 2016.
8. S. M. J. R. Fatemi, N. R. Abjadi, J. Soltani and S. Abazari, Speed sensorless control of a six-phase induction motor drive using backstepping control, IET Power Electronics, vol. 7, no. 1, pp. 114-123, 2014.
9. M. Bermúdez, H. Guzmán, I. González-Prieto, F. Barrero, M. J. Durán and X. Kestelyn, Comparative study of DTC and RFOC methods for the open-phase fault operation of a 5-phase induction motor drive, IECON 2015 - 41st Annual Conference of the IEEE Industrial Electronics Society, Yokohama, Japan, November 2015, Proc. pp 002702-002707.
10. M. Bermúdez, I. González-Prieto, F. Barrero, H. Guzman, X. Kestelyn and M. Duran, An Experimental Assessment of Open-Phase Fault-Tolerant Virtual Vector Based Direct Torque Control in Five-Phase Induction Motor Drives, *IEEE Trans. on Power Electronics*, vol. PP, no. 99 , pp. 1-1, 2017.
11. M. J. Duran, I. Gonzalez-Prieto, N. Rios-Garcia and F. Barrero, A Simple, Fast and Robust Open-phase Fault Detection Technique for Six-phase Induction Motor Drives, *IEEE Trans. on Power Electronics*, vol. 33, no. 1 , pp. 547-557, 2018.
12. H. Rahali, S. Zeghlache and L. Benalia, Adaptive Field-Oriented Control Using Supervisory Type-2 Fuzzy Control for Dual Star Induction Machine, International Journal of Intelligent Engineering and Systems, vol. 10, no. 4, pp. 28-40, 2017.
13. A. Meroufel, S. Massoum, A. Bentaallah, P. Wira, F. Z. Belaimeche and A. Masssoum, double star induction motor direct torque control with fuzzy sliding mode speed controller, Rev. Roum. Sci. Techn.–Électrotechn. et Énerg., vol. 62, no. 1, pp. 26-35, 2017.

14. Z. Tir, Y. Soufi, M. N. Hashemnia, O. P. Malik and K. Marouani, Fuzzy logic field oriented control of double star induction motor drive, Electrical Engineering, vol. 99, no. 2, pp. 495-503, 2017.
15. S. Lekhchine, T. Bahi and Y. Soufi, Indirect rotor field oriented control based on fuzzy logic controlled double star induction machine, International Journal of Electrical Power & Energy Systems, vol. 57, pp. 206-211, 2014.

Appendix

Machine parameters

$R_{s1} = R_{s2} = 3.72\ \Omega$ Stator1, Stator2 resistance respectively.

$L_{s1} = L_{s2} = 0.022$ H Stator1, Stator2 inductance respectively.

$R_r = 2.12\ \Omega$ Rotor resistance.

$L_r = 0.006$ H Rotor inductance.

$L_m = 0.3672$ H Mutual inductance.

$J = 0.\ 0625\ Kgm^2$ Inertia.

$K_f = 0.001\ Nm.\ (rd/s)^{-1}$ damping coefficient.

$p = 1$ Number of pole pairs.